UCLA

Title

Crystal structure of a conformational antibody that binds tau oligomers and inhibits pathological seeding by extracts from donors with Alzheimer's disease.

Permalink

Journal

ISSN

Authors

Abskharon, Romany
Seidler, Paul M
Sawaya, Michael R
et al.

Publication Date

DOI

Copyright Information

Peer reviewed

Crystal structure of a conformational antibody that binds tau oligomers and inhibits pathological seeding by extracts from donors with Alzheimer's disease

Romany Abskharon[1,2,‡] ![ORCID], Paul M. Seidler[1,2,‡] ![ORCID], Michael R. Sawaya[1,2] ![ORCID], Duilio Cascio[1,2], Tianxiao P. Yang[1,2], Stephan Philipp[3], Christopher Kazu Williams[4], Kathy L. Newell[5] ![ORCID], Bernardino Ghetti[5] ![ORCID], Michael A. DeTure[6] ![ORCID], Dennis W. Dickson[6], Harry V. Vinters[4,7], Philip L. Felgner[8] ![ORCID], Rie Nakajima[9], Charles G. Glabe[3], and David S. Eisenberg[1,2,*] ![ORCID]

From the [1]Departments of Chemistry and Biochemistry and Biological Chemistry, UCLA-DOE Institute, UCLA, Los Angeles, California, USA, the [2]Howard Hughes Medical Institute, UCLA, Los Angeles, California, USA, the [3]Department of Molecular Biology and Biochemistry, University of California, Irvine, California, USA, the [4]Department of Pathology & Laboratory Medicine, David Geffen School of Medicine at UCLA, Los Angeles, California, USA, the [5]Department of Pathology and Laboratory Medicine, Indiana University School of Medicine, Indianapolis, Indiana, USA, the [6]Department of Neuroscience, Mayo Clinic, Jacksonville, Florida, USA, the [7]Department of Neurology, David Geffen School of Medicine at UCLA, Los Angeles, California, USA, the [8]Vaccine Research and Development Center, Department of Physiology and Biophysics, University of California Irvine, Irvine, California, USA, and the [9]Vaccine Research and Development Center, Department of Physiology and Biophysics, University of California Irvine, Irvine, California, USA

Edited by Paul E. Fraser

Soluble oligomers of aggregated tau accompany the accumulation of insoluble amyloid fibrils, a histological hallmark of Alzheimer disease (AD) and two dozen related neurodegenerative diseases. Both oligomers and fibrils seed the spread of Tau pathology, and by virtue of their low molecular weight and relative solubility, oligomers may be particularly pernicious seeds. Here, we report the formation of *in vitro* tau oligomers formed by an ionic liquid (IL15). Using IL15-induced recombinant tau oligomers and a dot blot assay, we discovered a mAb (M204) that binds oligomeric tau, but not tau monomers or fibrils. M204 and an engineered single-chain variable fragment (scFv) inhibited seeding by IL15-induced tau oligomers and pathological extracts from donors with AD and chronic traumatic encephalopathy. This finding suggests that M204-scFv targets pathological structures that are formed by tau in neurodegenerative diseases. We found that M204-scFv itself partitions into oligomeric forms that inhibit seeding differently, and crystal structures of the M204-scFv monomer, dimer, and trimer revealed conformational differences that explain differences among these forms in binding and inhibition. The efficiency of M204-scFv antibodies to inhibit the seeding by brain tissue extracts from different donors with tauopathies varied among individuals, indicating the possible existence of distinct amyloid polymorphs. We propose that by binding to oligomers, which are hypothesized to be the earliest seeding-competent species, M204-scFv may have potential as an early-stage diagnostic for AD and tauopathies, and also could guide the development of promising therapeutic antibodies.

Alzheimer's disease (AD) is the most common neurodegenerative disorder, affecting nearly 50 million individuals world-wide, with no effective treatment or therapy even to slow disease progression (1). AD is associated with the accumulation of extracellular plaques composed of Aβ peptides, and intracellular neurofibrillary tangles of hyperphosphorylated Tau protein (2). Although the cascade of molecular events that leads to AD is not fully understood, the spreading of tau pathology through the brain tracks with cognitive decline (3), and small oligomers and fibrillar inclusions are thought to drive the spread of tau pathology by seeding (4). Besides AD, numerous other neurodegenerative disorders are associated with the deposition of aggregated tau in the brain. Referred to as tauopathies, these include chronic traumatic encephalopathy (CTE), frontotemporal dementia with parkinsonism-17 (FTDP-17), progressive supranuclear palsy, and Pick's disease among others (5, 6). Tauopathies are distinguished from AD by an absence of fibrillar inclusions of β-amyloid, although tau pathology is thought to progress in both by the seeded spreading of aggregated tau from cell to cell in a prion-like manner (7).

Oligomeric inclusions of soluble tau could form prior to the deposition of larger neurofibrillary tangles in the brain, and soluble oligomers have been shown to provoke neuronal toxicity and accumulation of fibrillar tau inclusions (8–11). Supporting the hypothesis that soluble oligomers are neurotoxic, stereotaxic subcortical injections of tau oligomers into WT mice induced measurable neurodegeneration by interfering with mitochondrial and synaptic functions (12–15). Similarly, other studies have shown that recombinant tau oligomers impair memory and long-term potentiation by seeding the spread of tau pathology and neurodegeneration (16–18).

Our laboratory has previously used a structure-based approach to design inhibitors targeting three amyloidogenic segments of tau, SVQIVY, VQIVYK, and VQIINK. These inhibitors are capable of blocking tau aggregation, and underscore the important role of these segments in driving tau aggregation and seeding

---

This article contains supporting information.
‡ These authors contributed equally to this work.
* For correspondence: David S. Eisenberg, david@mbi.ucla.edu.

(19–23). Taking a different approach to inhibitor design, others have exploited tau antibodies that bind various epitopes and inhibit seeding. Passive immunization with anti-tau oligomer antibodies called "tau oligomer mAb" (TOMA) reduced levels of tau oligomers and reversed locomotor and memory deficits in tau P301L mice, suggesting that antibodies that target tau oligomers may be effective therapeutics for AD and various tauopathies (24).

Here we report that a novel inducer of tau aggregation: ionic liquid 15 (IL15), promotes the formation of prefibrillar tau oligomers that can be isolated for biochemical studies. Using IL15-induced oligomers of tau-K18, we discovered that a monoclonal rabbit antibody (M204) that was purified from A11 polyclonal serum binds to oligomeric tau, but not to recombinant monomers or fibrils (25). We engineered a single-chain variable fragment (scFv) construct of M204 and found that it too forms oligomers of different molecular weights, and that M204-scFv inhibits seeding by isolates from the autopsied brains of human donors with AD and CTE. Structures of the scFv M204 monomer, dimer, and trimer reveal differences in the antigen-binding loops, suggesting a structural basis for the enhanced inhibition of tau seeding by oligomeric forms of the scFv antibody.

Results

Oligomer formation

To produce prefibrillar, seeding-competent oligomers of tau, we sought new inducers of aggregation. Because classic aggregation inducers, heparin and arachidonic acid, yield fibrillar aggregates too rapidly to permit isolation of oligomeric intermediates of aggregated tau, we surveyed a panel of 24 ionic liquids to find slower inducers of aggregation using a thioflavin T (ThT) assay (Fig. 1A, Fig. S1). We turned to ionic liquids (IL) because many aggregation catalysts of tau are charged molecules, and ILs are reported to alter the solubility of other amyloid proteins and fibrils (26–28). Our initial work was on the 129-residue microtubule-binding domain of tau, known as tau-K18 (29). Of the 24 ionic liquids screened, two induced tau-K18 aggregation: 50% (w/v) 1-*n*-butyl-3-methylimidazolium *n*-octylsulfate (IL15) and 50% (w/v) triisobutylmethylphosphonium tosylate (IL23). IL15 catalyzed aggregation of tau-K18 more robustly than IL23, but with a lag time that was about 5 times longer than heparin-induced aggregation. The slower kinetics of IL15-induced aggregation allowed us to isolate oligomers during a short kinetic window, referred to as the oligomer extraction window, which corresponds to the early appearance of the ThT signal (Fig. 1A). Reducing the rate of aggregation seems to be an effective way of forming tau oligomers because it was also shown that oligomers of tau can be isolated and chemically stabilized by aggregation at 4 °C (30).

IL15-induced oligomers of tau-K18 isolated during the oligomer extraction window were purified by size exclusion chromatography (SEC) (Fig. 1B) and tested for immunoreactivity and seeding. As shown in Fig. 1C, the tau-K18 oligomer peak reacted with the polyclonal antisera A11, previously shown to be conformation-specific for amyloid oligomers (31), whereas the monomer tau-K18 peak showed no A11 immuno-

reactivity. These results agree with other studies that show the A11 antibody binds to a common structural motif in amyloid oligomers (31, 32). Electron micrographs of the oligomer peak fraction revealed a mixture of protofilaments, spherical or disk aggregates that were 10-20 nm in diameter, and apparent mixtures of the two, which as shown in *inset 1* of Fig. 1E, resemble spherical aggregates with emerging protofilaments. By contrast, the monomer fraction was mostly devoid of apparent aggregates (Fig. 1D). When incubated with IL15 for longer times, ThT fluorescence signal plateaued and electron micrographs revealed fibrillar aggregates that display cross-β diffraction (Fig. 1, F and G), suggesting that the end point aggregates that are formed by IL15 are fibrils.

Seeding by tau-K18 oligomers was measured in HEK293 tau biosensor cells that express YFP-tagged tau-K18 (33). As shown in Fig. 1, H–K, tau-K18 oligomers purified by SEC robustly seed aggregation in tau biosensor cells, whereas tau-K18 from the monomer peak shows no seeding activity. End point tau-K18 fibrils induced by IL15 also seeded biosensor cells at a level similar to the purified tau-K18 oligomers (Fig. S2).

M204 antibody binding to tau oligomers

As an alternative to A11 polyclonal antisera, we sought a mAb that would be more amenable to protein engineering, because antibody variants can exhibit different *in vivo* and therapeutic efficacies (33). Using purified preparations of IL15-induced tau-K18 oligomers, we screened a panel of monoclonal antibodies to find one that specifically recognized the oligomer, and could thus be used to engineer single-chain antibodies. We previously discovered a rabbit mAb derived from A11-producing rabbits called M204 that, like A11, recognizes oligomeric but not fibrillar conformations of amyloidogenic proteins (25). Dot blots immunostained with M204 reveal strong immunoreactivity to SEC fractions containing the IL15-induced tau-K18 oligomer, but no immunoreactivity to SEC fractions containing the tau-K18 monomer (Fig. 2, B and C, and Fig. S3). In addition, neither recombinant fibrils of full-length tau (tau40) nor purified tau40 had any immunoreactivity with M204 on the same immunoblot (Fig. 2C). Next, we analyzed binding of M204 to recombinant oligomers of tau-K18 and tau40 by ELISA. As shown in Fig. 2, D–F, M204 reacted with fractions containing both tau-K18 and tau40 oligomers, but not fractions containing monomers of either tau construct.

To determine which tau sequences are recognized by the M204 antibody, we performed epitope mapping using an array of overlapping tau peptides. As shown in Fig. 3A, M204 bound the aggregation-driving segments VQIINK and SVQIVY more strongly than neighboring regions. These results suggest M204-tau oligomer recognition is mediated by the steric-zipper forming segments that drive tau aggregation, and suggest that these segments are presented differently in the oligomer conformation compared with the conformations of the monomer and recombinant fibril.

Because M204 recognizes epitopes of prefibrillar structures that are important for tau aggregation, we asked if antibody binding inhibits seeding by IL15-induced tau oligomers. To test this, we measured seeding and inhibition in HEK293 tau

§ASBMB

J. Biol. Chem. (2020) 295(31) 10662–10676 **10663**
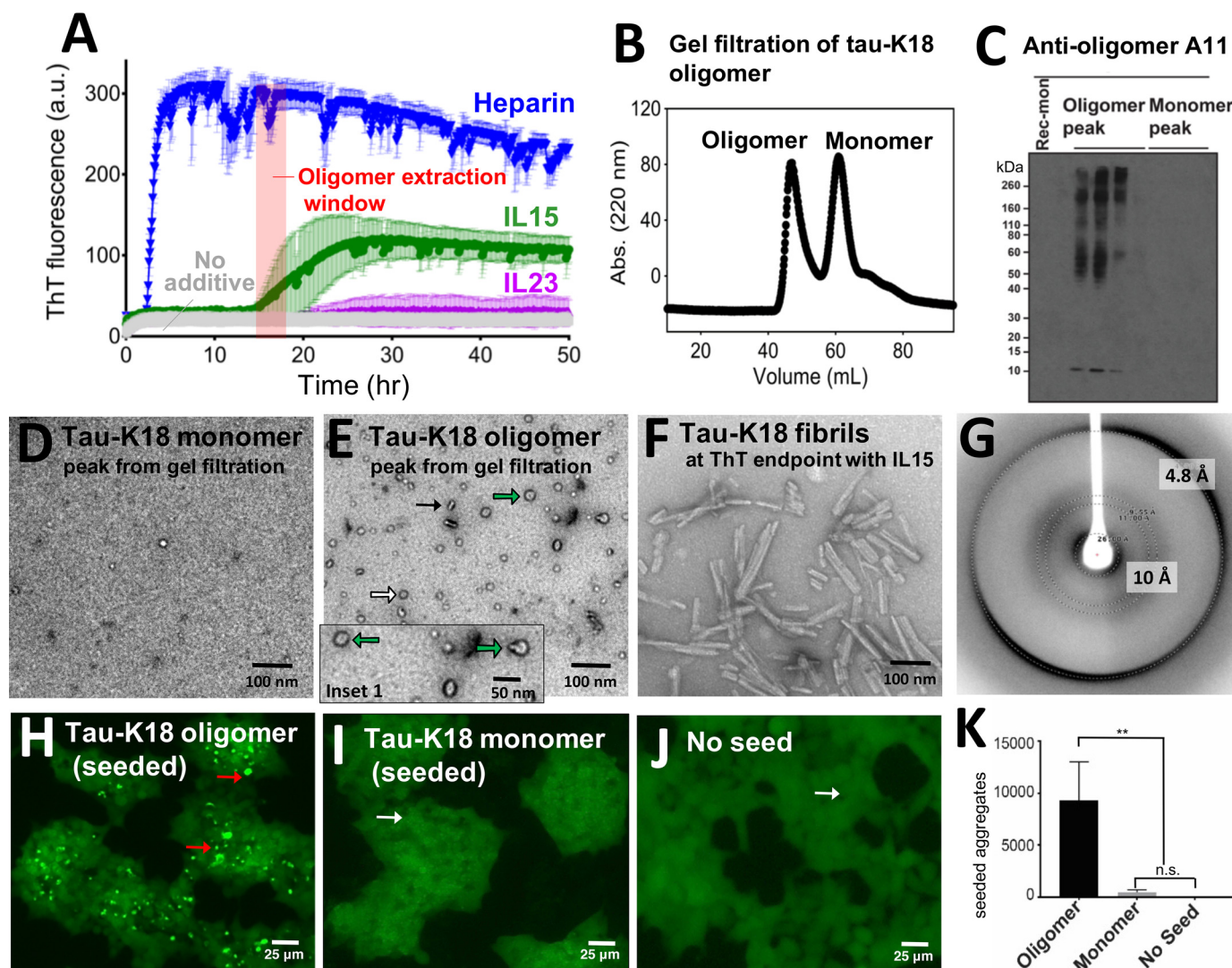
Figure 1. IL15 induces formation of tau-K18 oligomers and amyloid fibrils. *A,* aggregation kinetics of tau-K18 induced with 0.225 mg/ml of heparin (*blue*), 2% (w/v) IL15 (*green*), or 2% (w/v) IL23 (*magenta*), measured by fluorescence of ThT dye at 480 nm. *B,* separation of tau-K18 monomer and oligomer after 16-18 h of incubation and shaking with IL15, as in *A,* by SEC using a HiLoad 16/600 Superdex 75 pg column. *C,* immunoblot analysis of tau-K18 oligomer and monomer fractions from the SEC peaks using anti-oligomer A11 polyclonal antibody. *D–F,* negative stain electron micrographs of tau-K18 (*D*) monomer, (*E*) oligomer, and (*F*) fibril prepared with IL15. *G,* X-ray fibril diffraction from tau-K18 fibrils prepared with IL15. *H,* HEK293 tau biosensor cells expressing YFP-tagged tau-K18 and seeded with 1.5 nM tau-K18 oligomer. *I,* as in *H,* except seeded with 1.5 nM tau-K18 monomer. *J,* HEK293 tau biosensor cells without addition of tau seed. Representative cells that contain aggregates are marked by *red arrows,* and cells without by *white arrows. K,* quantification of seeding from representative images shown in *H–J.* Statistical analysis was performed using a one-way ANOVA (**, $p < 0.005$, *n.s.,* no significance) and Tukey's multiple comparison in GraphPad Prism. *Error bars* show the S.D. of three replicates.

biosensor cells (34). As shown in Fig. 3, *B–D,* IL15-induced tau-K18 oligomers strongly seeded aggregation in tau biosensor cells, and seeding was inhibited by the addition of purified 10 μM M204.

Next, we sought to determine whether AD brain-derived tau was immunoreactive to M204. We found M204 immunoreactivity in both the crude and Sarkosyl-insoluble fractions of an extract from the brain of a donor with AD, however, the immunoreactivity was markedly stronger in the crude and Sarkosyl-soluble fractions compared with the Sarkosyl-insoluble fraction (Fig. 3E and Fig. S4). Consistent with previous data showing that A11 does not stain large fibrils from AD tissue (31), no immunoreactivity was found in the same tissue probed with A11. Because A11 is polyclonal, the amount of M204-like antibody in the A11 antiserum may be too low to detect low levels

of oligomers that could be present in the AD tissue. These data suggest that small concentrations of oligomer in AD tissue that are not detected by A11 may be detected using M204.

Design of the single-chain M204 antibody

Because M204 is an inhibitor of tau seeding and shows immunoreactivity with AD brain extract, we aimed to engineer a single-chain (scFv) version of the antibody, which because of its smaller size, may possess greater tissue penetration than the full-length antibody (35). As shown in Fig. 4, the scFv construct is a small antibody of 247 residues generated by connecting the variable regions of the heavy (VH) and light chains (VL) of Igs using a flexible linker (36). Others have reported that scFvs are limited in expression due to misfolding and formation of inclusion bodies and loss of binding
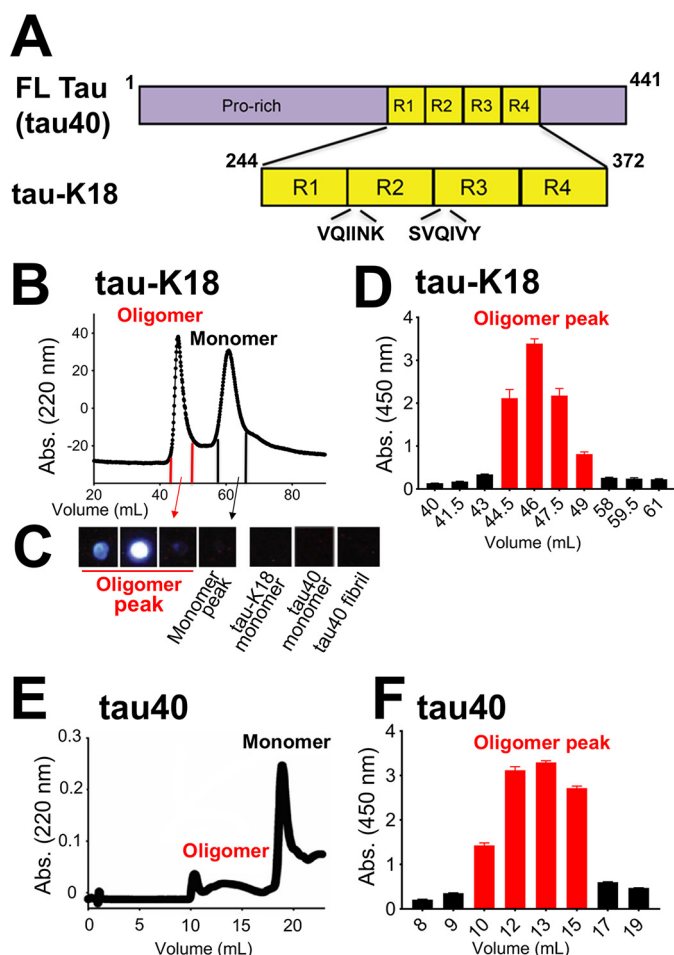
Figure 2. Tau oligomer purification and antibody binding. *A,* schematic representation of full-length tau (tau40) and the tau-K18 construct containing the microtubule binding domains R1–R4. *B,* S75 16/600 SEC purification of tau-K18 oligomer prepared as described in the legend to Fig. 1 with IL15. *C,* dot blot of chromatographed tau-K18 oligomer and monomer fractions (*left set of four*), and of purified tau-K18 monomer, tau40 monomer, and tau40 fibril (*right set of 3*). Only the oligomer peak shows immunoreactivity with M204. *D,* ELISA showing immunoreactivity of monoclonal M204 antibody with chromatographed S75 fractions containing tau-K18 oligomer (fractions 44-49, colored *red*), but not tau monomer (fractions 58-61, colored *black*). A volume of 20 μl of the indicated SEC fraction was diluted into 100 μl of coating buffer and applied to ELISA plate. In fractions 46 and 61 (the highest peaks), 20 μl = 100 ng of protein/well. *E,* S200 10/300 SEC purification of oligomeric tau40 prepared with IL15. *F,* ELISA showing immunoreactivity of monoclonal M204 with chromatographed S200 fractions containing tau40 oligomer (fractions 10-15, colored *red*) but not tau monomer (fractions 17-19, colored *black*). A volume of 50 μl of the indicated SEC fraction containing tau40 oligomer (fractions 8-15) were diluted into 100 μl of coating buffer. For tau40 monomer fractions 17 and 19, 10 μl was used to coat ELISA plates rather than 50 μl because the peak monomer fraction was about 5 times the intensity of the oligomer peak. For reference, the amount of protein used to coat the ELISA plate in fractions 13 and 19 (the highest peaks) was 100 ng of protein. *Error bars* show the S.D. of triplicate measurements.

activity in the bacterial cytoplasm (37, 38). To overcome this limitation, we fused the M204-scFv to a PelB leader sequence to shuttle the protein to the bacterial periplasm. Using this expression system, we achieved 1-2 mg yields of purified protein per liter of bacteria.

SEC of purified M204-scFv revealed different oligomer forms: monomer, dimer, and trimer (Fig. 4C). It has been reported that scFv antibodies may form dimers depending on the sequence of the antibody and/or the flexible linker (39, 40). We tested the pos-

sibility that M204-scFv forms intermolecular disulfide bonds that stabilize the oligomer by comparing the mobility of purified M204-scFv by reducing and nonreducing SDS-PAGE (Fig. 4D). Under reducing conditions, the M204-scFv proteins that eluted from the SEC as monomers, dimers, and trimers all migrated with similar mobility by SDS-PAGE. However, nonreducing conditions revealed distinct high molecular weight bands for the dimer and trimer SEC fractions, suggesting that the dimer and trimer species are disulfide linked. Notably the dimer species is the stronger band in both the dimer and trimer lanes, suggesting the dimer is the more stable of the oligomeric scFv species. That, and the appearance of monomer in the dimer and trimer lanes (Fig. 4D, *seventh and 11th lanes*), along with the appearance of some potential dimer in the monomer fraction (*lane* 3) suggests that there exists some degree of interconversion among scFv oligomers, potentially complicating biochemical analyzes of the different M204-scFv oligomer species. Nevertheless, these data demonstrate that different oligomeric forms of M204-scFv can be enriched.

We compared the tau immunoreactivity of the different M204-scFv oligomers by ELISA. All three M204-scFv species recognized tau-K18 oligomer, and none recognized the tau-K18 monomer, indicating that the engineered scFv has the same specificity as the mAb for tau oligomers (Fig. 5, *A–D*, and Fig. S5). M204-scFv dimer and trimer showed higher binding signals for tau oligomers compared with the monomer, suggesting that the M204-scFv dimer and trimer might have better potential to bind and inhibit tau oligomers.

M204-scFv inhibits aggregation recombinant tau

To test the ability of M204-scFv to inhibit the primary aggregation of tau, we added different ratios of M204-scFv monomer, dimer, and trimer to tau-K18 monomer, and measured aggregation using an *in vitro* ThT assay. All of the M204-scFv antibodies delayed fibril formation at ratios of 1:1 and 1:0.5 (tau-K18:scFv) (Fig. 5, *E–G*). However, the M204-scFv dimer exhibited the most pronounced delay in lag time, whereas the M204-scFv monomer showed the smallest effect. The delay in tau fibril formation was somewhat unexpected as neither monoclonal M204 nor the M204-scFvs showed binding to either recombinant tau fibrils or monomers. These results suggest that tau oligomers may be formed transiently during the fibrillization, and we speculate that these prefibrillar tau-K18 oligomers could thus become the target of M204 inhibition.

To determine whether our M204-scFv antibodies are inhibitors of seeding by tau fibrils from pathological tissues, we tested the seeding and inhibition of fibrils that were extracted from AD brain tissue. Electron micrographs of extracted fibrils from one representative AD donor confirms that the Sarkosyl-insoluble fraction contains an abundance of fibrils, but without apparent oligomers (Fig. 6A). Nevertheless as shown in Fig. 6, *B–F*, dimers and trimers of M204-scFv block seeding by extracts from three different AD donors. M204-scFv monomer on the other hand is a poor inhibitor of seeding, and in one case, even stimulates seeding (Fig. 6C).
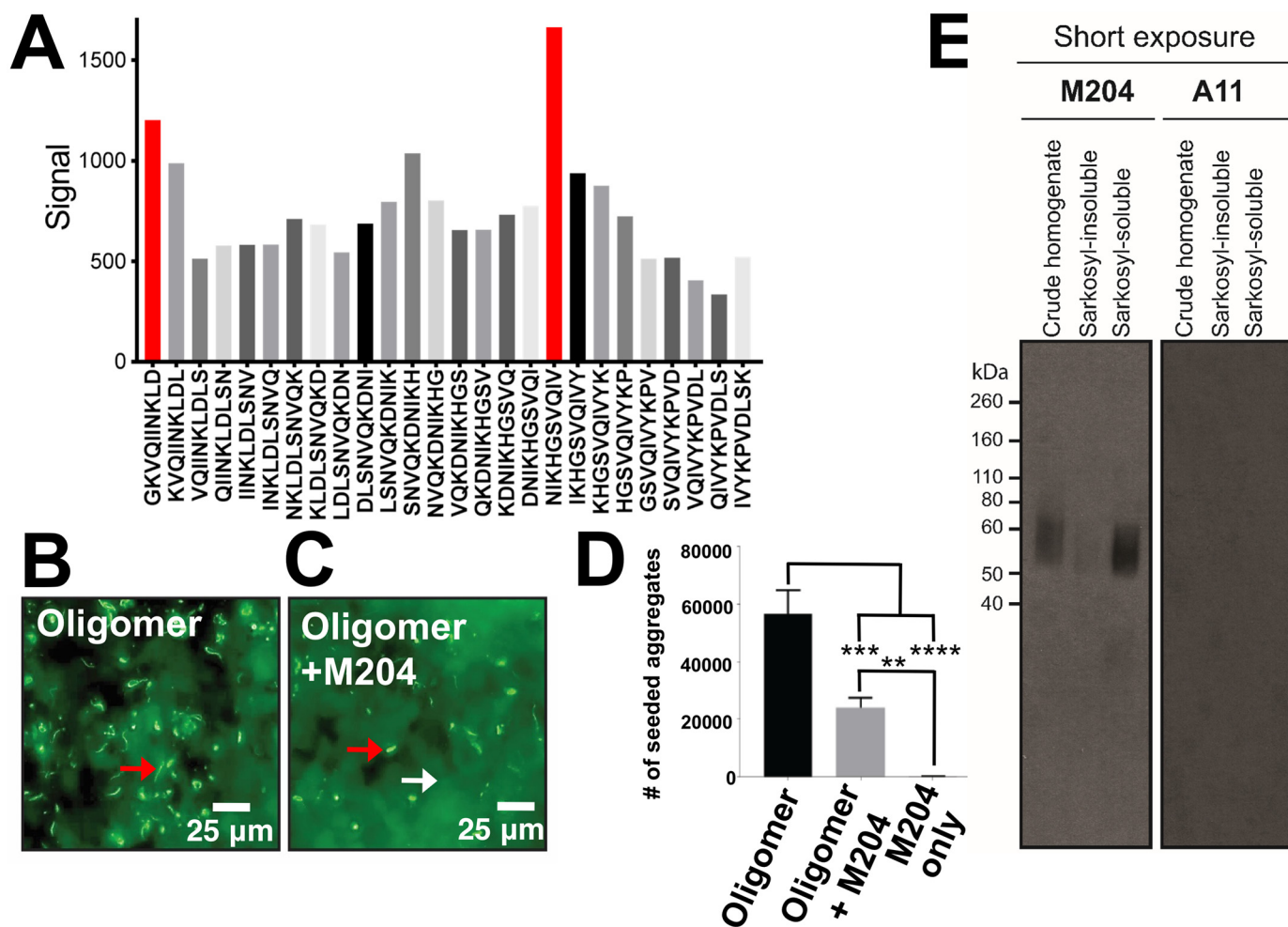
Figure 3. M204 binds to aggregation-driving segments in synthetic, recombinant tau and AD brain-derived tau. *A,* epitope mapping using a peptide array with overlapping synthetic tau peptides shows M204 binding most strongly to peptides containing the sequences KVQIINK and SVQIVY (in *red*). *B,* seeding by IL15-mediated tau-K18 purified oligomers in HEK293 biosensor cells expressing YFP-tagged tau-K18. *C,* as in *B,* except following treatment of tau-K18 oligomer with 10 μM M204 antibody. Seeding inhibition by M204 is interpreted based on the appearance of fewer puncta compared with *B.* Representative cells containing aggregated tau are marked by *red arrows,* and cells without by *white arrows. D,* quantification of seeding from representative images shown in *B* and *C.* Tau oligomer seeding and inhibition by M204 antibody were determined by calculating the number of normalized puncta per well of a 96-well–plate. Statistical analysis was performed using one-way ANOVA (****, $p < 0.0001$; ***, $p < 0.0006$; **, $p < 0.003$) and Tukey's multiple comparison in GraphPad Prism. *Error bars* show the S.D. of three replicates. *E,* Western blotting of tissue from the brain of a donor with AD, fractionated into: crude brain homogenate, Sarkosyl-insoluble, and Sarkosyl-soluble fractions, each probed with M204 or A11 anti-oligomer antibodies.

Because we hypothesized that brain regions affected at different stages of disease could contain different species of aggregated tau, for Donor 3 we elected to test seeding by extracts from two different brain regions: the hippocampus, which exhibits tau aggregation at early-to-moderate stages of AD (41) (Fig. 6*D*), and the occipital lobe, which is affected at later stages of AD (Fig. 6*E*). Nevertheless, inhibition of seeding inhibition by extracts from both brain regions was virtually identical.

Collectively our results suggest that although M204-scFv preferentially targets recombinant oligomers over recombinant fibrils of tau, the antibody somehow still inhibits seeding by pathological brain extracts that are enriched in tau fibrils. It is possible that oligomers present in the pathological brain extracts are too small to be observed in negative stain electron micrographs, or that the epitopes presented on fibrils from pathological brain extracts more closely resembles the epitope fingerprint of the recombinant oligomers that are produced using IL15. Additionally, it is possible that seeding by patholog-

ical brain extracts is mediated mostly by small oligomers that are generated by sonicating the fibrils prior to seeding, and that these oligomers are the target of M204-scFv inhibition.

As a further test of the inhibitory power of dimers and trimers of M204-scFv, we assayed inhibition of seeding by crude lysates from four additional donors with diagnosed tauopathies: two with CTE, one with CBD, and one with a familial (P301L) mutation. As shown in Fig. 7, M204-scFv blocked seeding by one of the two CTE donors, but not by extracts from donors with CBD or the P301L mutation. In fact seeding by CBD or the P301L extracts appeared to be marginally enhanced by M204-scFv. This finding was unexpected given our result that M204-scFv potently inhibits seeding by fibrils from the Sarkosyl-insoluble fraction of three AD donors. As we discuss below, this apparent contradiction could be explained by the interaction of M204-scFv with different disease-associated polymorphs in a way that in one case (as in AD) inhibits seeding, but in other cases enhances the internalization of the seed.
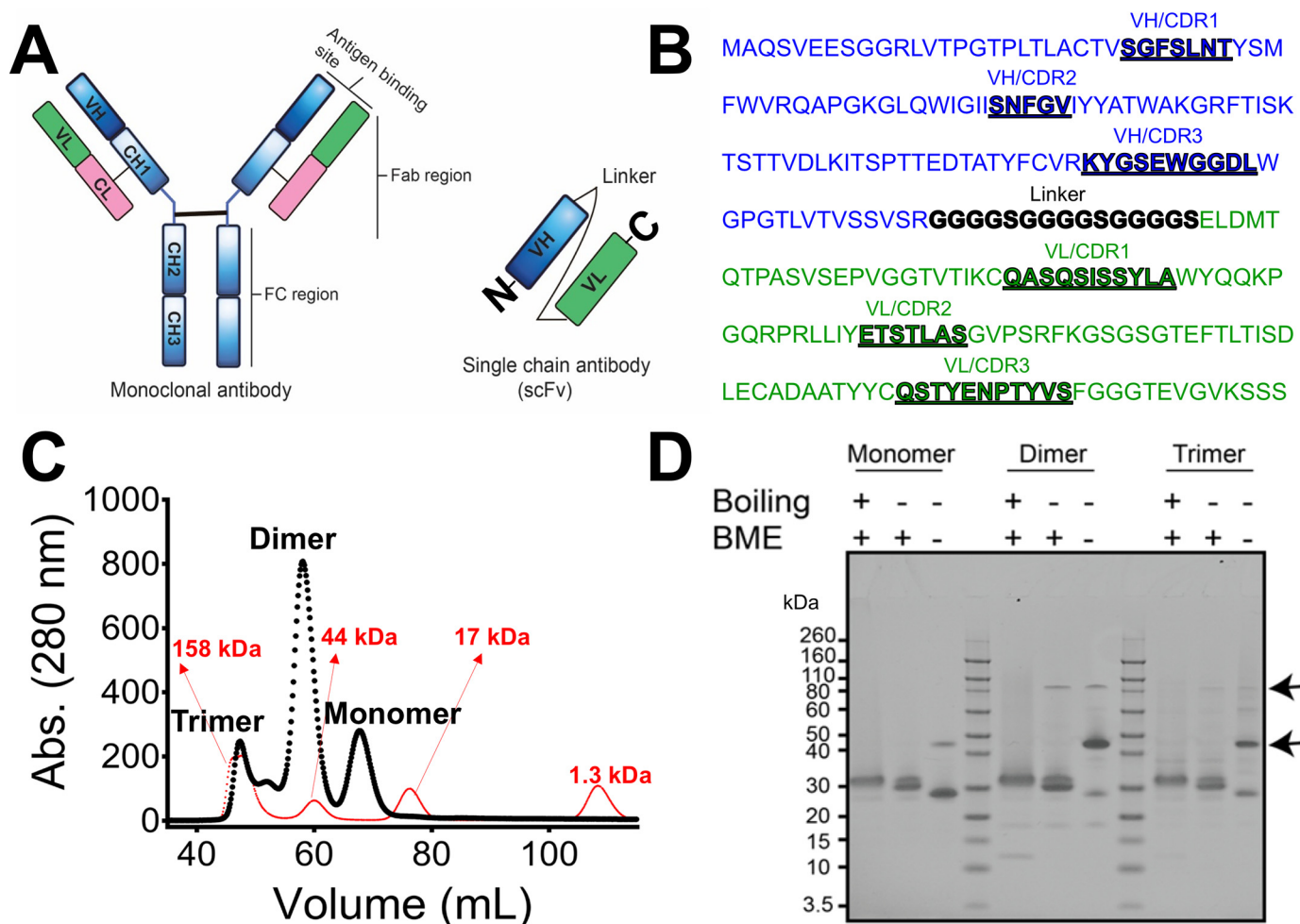
Figure 4. M204-scFv purifies as a mixture of monomer and oligomers. *A,* schematic comparing a full-length mAb and the scFv fragment. *B,* sequence of M204-scFv. The VH and VL variable domains are colored *blue* and *green*, respectively, and the sequences of the CDRs loops are *bolded* and *underlined*. The VH and VL fragments are connected by a flexible linker with sequence (Gly$_4$Ser)$_3$. *C,* S75 SEC of M204-scFv overlaid with gel filtration standards (in *red*) showing apparent monomer, dimer, and trimer M204-scFv species, as judged by comparison to the SEC protein standards. *D,* SDS-PAGE analysis of monomeric, dimeric, and trimeric M204-scFv fractions, run under reducing and nonreducing conditions, as indicated, showing high molecular weight bands that correspond to the dimeric and trimeric species (marked by *black arrows*) under nonreducing conditions.

X-ray crystal structure of the M204-scFv monomer, dimer, and trimer

To understand the structural basis of M204-scFv oligomerization into a functionally active inhibitor of seeding, we determined the X-ray crystal structures of the M204-scFv monomer, dimer, and trimer conformations (Table 1). The structures of all of the M204-scFv antibodies adopt a characteristic immunoglobulin (Ig)-fold, having one variable domain from both the L and H chains per protomer (Fig. 8). Each variable domain has three CDR loops (CDR1, CDR2, and CDR3) in both the heavy (H) and light (L) domains (Fig. 8A). The dimer interface is formed by a face opposite the antigen-binding surface, and the same interface comprises one of the two intermolecular interfaces formed by the M204-scFv trimer (Fig. 8, B and C). Our crystal structures reveal that all of the CDR loops from both the L and H domains are surface exposed in all three structures: the monomer, dimer, and trimer. These structures suggest that trimeric and dimeric forms of M204-scFv have greater potential to bind to oligomeric tau because of the greater number of clustered antigen-binding loops that are present on the surface of the antibody in its oligomeric form.

CDR3 from both the H and L chains are generally believed to be the primary determinants of antigen binding (42). We carried out an alignment of all of the M204-scFv structures that we determined, and found that in one of the four molecules in the asymmetric unit of the dimer structure, CDR loop 3 (CDR3) of both the H and L chains adopt major conformational changes compared with the M204-FAB crystal structure determined previously (43), and the crystal structures of the monomer and trimer, which we determined in this work (Fig. 8, E and F). These data suggest that CDR3 possesses greater conformational flexibility in the dimeric and trimeric species, and by extension, potentially greater inhibition because of an improved ability of the antibody to interact with oligomeric tau. It is not apparent from our structures, however, why the dimeric and trimeric species would be afforded greater conformational flexibility.

Our analysis of the M204-scFv structures revealed that the dimer interface has potential to be stabilized by a disulfide bond, because Cys-202 from the two chains that form the dimer interface project toward each other, and are 3.4 Å apart
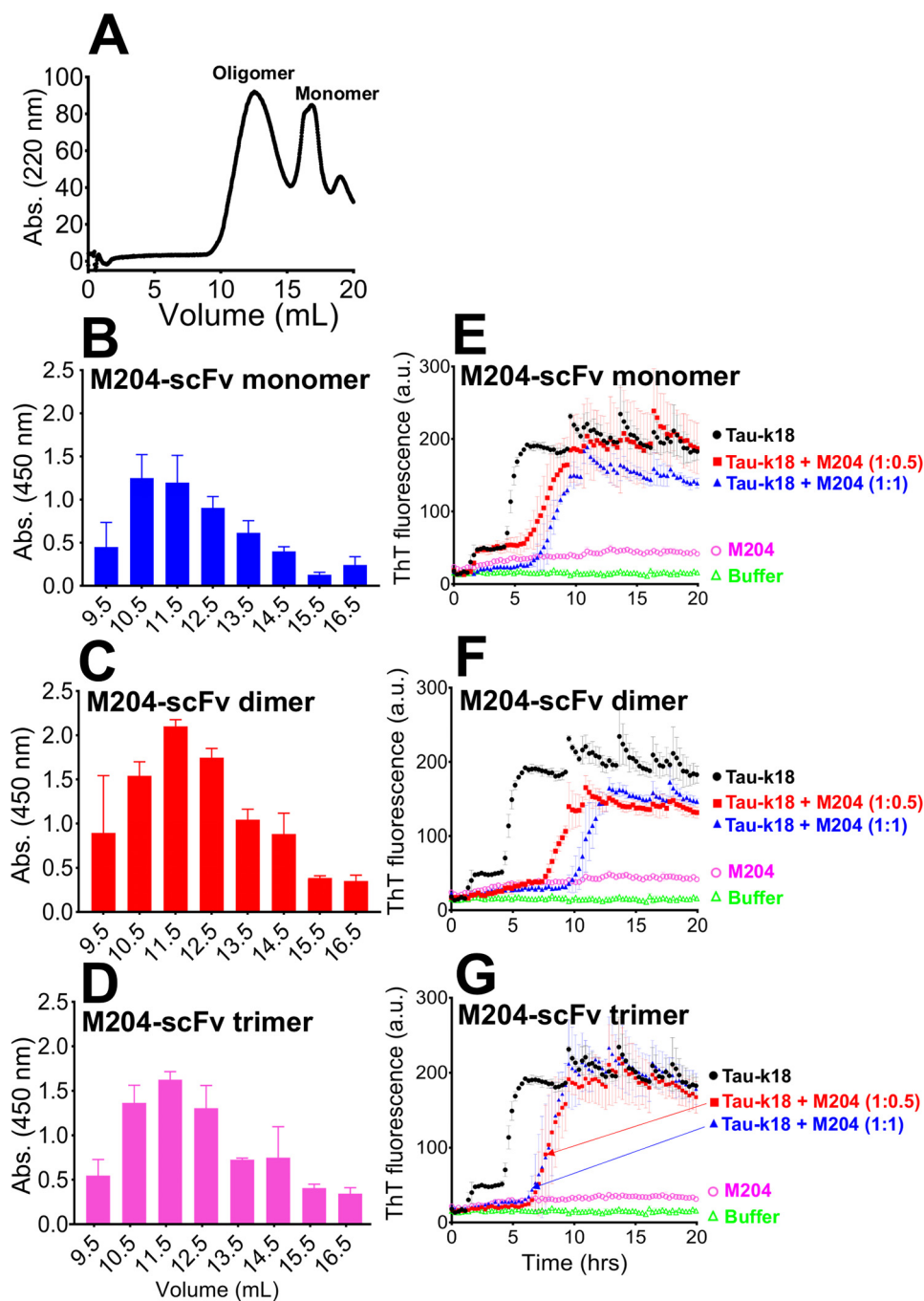
Figure 5. M204-scFv antibody delays *in vitro* aggregation. *A,* SEC purification of tau-K18 oligomer using a S200 10/300 column. The protein elution fractions were also monitored by absorption at 280 nm and presented in Fig. S7. *B–D,* ELISA showing immunoreactivity of the corresponding tau-K18 oligomer fractions from *A* with M204-scFv (*B*) monomer, (*C*) dimer, and (*D*) trimer. *E–G,* M204-scFv mediated inhibition of tau-K18 aggregation. Aggregation was measured by ThT fluorescence with M204-scFv added at molar ratios of 1:1 and 1:0.5 (tau-K18: M204-scFv), as indicated. Inhibition of IL15-induced tau aggregation by M204-scFv is shown for the M204-scFv monomer (*E*), dimer (*F*), and trimer (*G*). Tau-k18 is a positive control that was run in parallel but without the addition of M204-scFv, and is the same in aggregation experiments shown in *E–G*, colored *black*. *Error bars* represent the mean ± S.D. of three replicates.

in the crystal structures of both the dimer and trimer (Fig. 8*D*), although the disulfide appears to be reduced in both structures, potentially by X-ray–generated electrons (44, 45). The buried surface areas formed by the dimer and trimer are relatively low compared with other protein interaction interfaces, with a buried surface area of 581 Å^2 for the dimer and 379 Å^2 for trimer. These data suggest that the disulfide bond would likely be important for stabilizing the dimer conformation, and explains why the majority of M204-scFv purifies as a dimer (Fig. 4*C*).

Discussion

Here, we present a novel method of preparing reasonably stable oligomers of recombinant tau using IL15. Using these, we were able to pan libraries of monoclonal antibodies to identify M204, which binds IL15-induced tau oligomers, but not recombinant tau monomers or fibrils. By identifying monoclonal M204 as a conformation-selective antibody of tau oligomers, we were able to develop a single-chain antibody of M204 that recognizes recombinant tau oligomers with specificity that
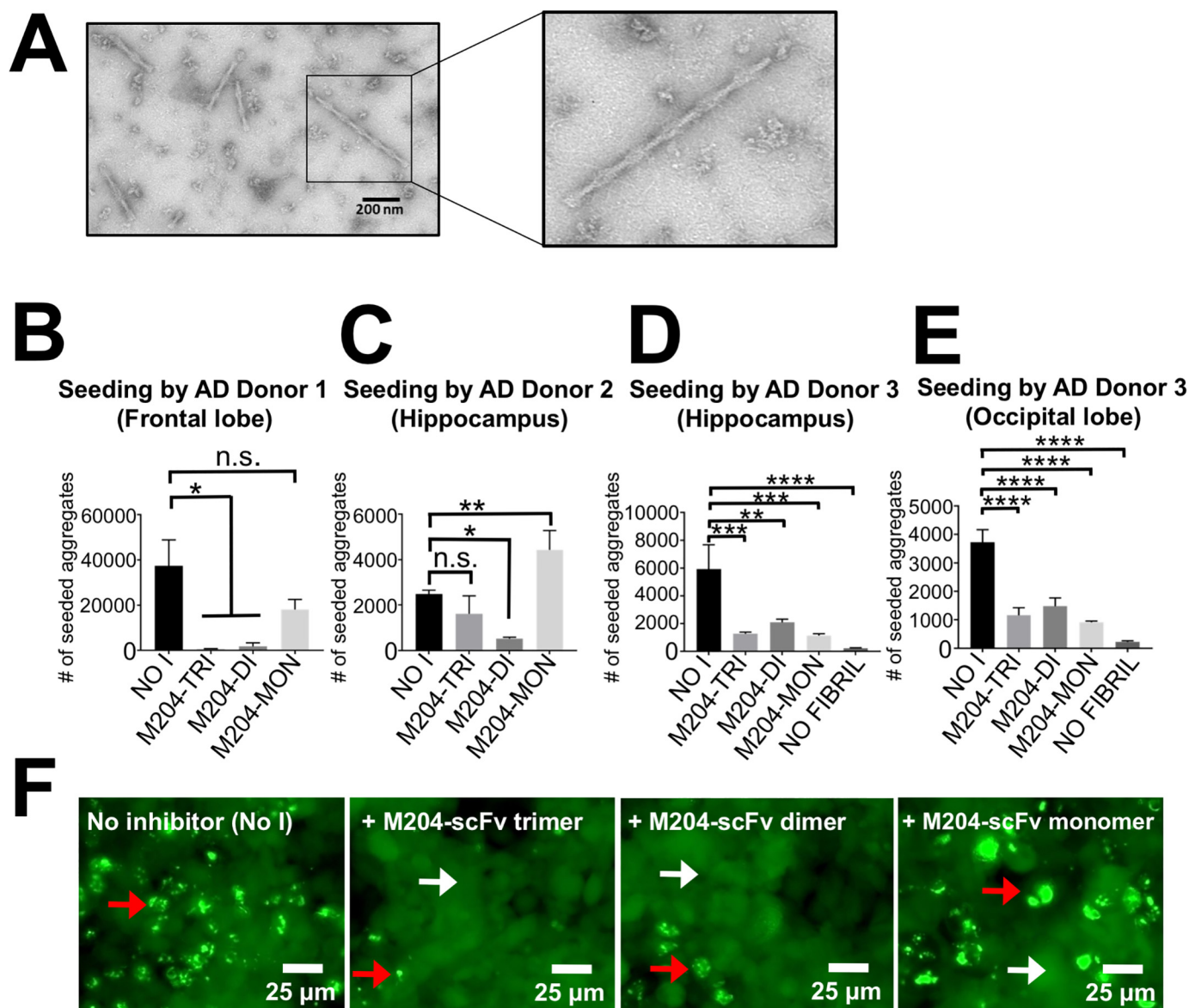
Figure 6. M204-scFv antibodies inhibit the seeding of tau aggregation by autopsied brain extracts from three human AD brain patients. *A,* negative stain electron micrograph of fibrils purified from human AD brain tissue. *Scale bar,* 200 nm. Zoom view shows a single fibril with a twist of two protofilaments, with the appearance of a paired helical filament. *B–E,* quantification of the inhibitory effect of M204-scFv antibodies on inhibition of seeding by Sarkosyl-insoluble fractions from AD brain tissue, measured in HEK293 biosensor cells expressing YFP-tagged tau-K18. Statistical analysis was performed using one-way ANOVA (****, $p < 0.0001$; ***, $p < 0.0002$; **, $p < 0.001$; *, $p < 0.01$, *n.s.*, no significance) followed by a Tukey's multiple comparison test in GraphPad Prism. *Error bars* show the S.D. of three replicates. *F,* representative images of seeding and inhibition in HEK293 biosensor cells expressing YFP-tagged tau-K18. Cells seeded with the Sarkosyl-insoluble fraction from AD Donor 1 without pre-treatment with M204-scFv (*left panel*) or no inhibitor (*No I*), and following overnight incubation with M204-scFv trimer, dimer, or monomer (as indicated). The seeding can vary dramatically from different regions of a given brain tissue section, and this reflects a naturally occurring nonuniform distribution of tau pathology in the brain. Representative cells that contain aggregates are marked by *red arrows,* and cells without by *white arrows.*

is similar to the parent mAb. The oligomers made using this approach exhibit hallmarks of prefibrillar intermediates, including immunoreactivity to the anti-amyloid oligomer antiserum A11 and proteopathic seeding.

Using IL15-induced tau oligomers and immunoreactivity with polyclonal antibody A11, we developed a related mAb (M204) that binds to recombinant tau oligomers. We find that M204 recognizes the aggregation-prone segments of tau with sequences VQIINK and SVQIVY. These segments are known to drive aggregation of tau, and inhibitors based on their structures inhibit fibril formation and seeding in biosensor cells (19). From M204, we engineered a single-chain antibody, M204-

scFv, which exhibits the same binding specificity as the mAb (M204). Because of their smaller sizes, single-chain antibodies have better potential to distribute into tissues compared with full-length antibodies (46). As such, the designed M204-scFv antibody may be useful as a starting point for the development of oligomer-based imaging agents and therapeutics.

The engineered M204-scFv antibody itself adopts three different self-associated species: a monomer, dimer, and trimer, all of which bind to recombinant tau oligomers, but with the dimer most effectively inhibiting seeding. Comparing the crystal structures of the M204-scFv monomer, dimer, and trimer reveals that CDR3 of both the H and L chains un-
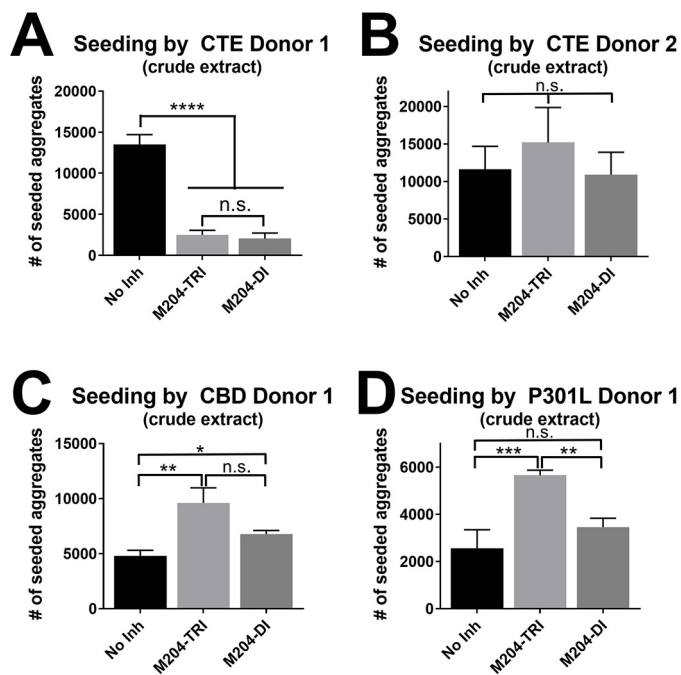
Figure 7. *A–D,* tests of the effectiveness of M204-scFv for inhibition of tau fibril seeding by diseased brain extracts in our HEK293 biosensor cell-based assay. M204-scFv dimer and trimer inhibit seeding by extract from (*A*) CTE Donor 1, but not (*B*) CTE Donor 2, (*C*) CBD donor, or (*D*) a donor with a P301L familial mutation. Statistical analysis was performed using one-way ANOVA (****, $p < 0.0001$; ***, $p < 0.0008$; **, $p < 0.005$; *, $p < 0.01$, *n.s.*, no significance) followed by a Tukey's multiple comparison test in GraphPad Prism. *Error bars* show the S.D. of three replicates.

dergo major conformation changes, in such a way that these loops may be more effective at epitope binding in the dimer than in monomer or trimer. In support of this, we find that the dimer produces the greatest oligomer-binding signal in our ELISA.

Our biochemical data suggest that the M204-scFv dimer is stabilized by a disulfide bond, and we suspect the disulfide is critical for the stability of the dimer, which has a buried surface area of 581 Å^2. The minimum buried surface area required to form a stable complex is around ~500 Å^2 (47). Therefore, the dimer interface is expected to be relatively weak; however, disulfide bonding would be expected to significantly reduce the off-rate of the complex. The crystal structure of the M204-scFv dimer shows Cys-202 from both protomers at a distance of 3.4 Å, and at 1σ contour level in the $2F_o - F_c$ map, the densities of the two Cys-202 from chains A and B touch, but do not appear to make continuous density that would be expected for a disulfide bond. On this basis, the disulfide appears to be broken in the crystal structure, potentially by X-ray–induced reduction. Given the proximity of these residues in the dimer interface, however, in addition to our biochemical data that suggest the dimer is both stable in solution, and is disulfide-mediated, we conclude that the dimer interface is likely to be fortified by a disulfide bond. The buried surface area of the trimer is much less, around 379 Å^2. We suspect the trimer is a less stable species. Accordingly, M204-scFv partitions mostly to the dimer conformation.

The lack of inhibition by M204 for some tauopathy brain extracts suggests the presence of various polymorphisms across

different tauopathies. That is, patients diagnosed with the different tauopathies may harbor different polymorphs of tau fibrils (48). CryoEM studies support this hypothesis, with different polymorphs occurring in AD brain compared with Pick's disease and CTE (49, 50). These results suggest that differences of pathological tau polymorphs may require the development of various different therapeutics to target the complex family of tauopathies (51). In addition, our inhibitor studies using crude brain extracts highlight other factors that may antagonize inhibition of tau seeding by M204-scFv, such as: 1) the presence of cellular proteases that could potentially degrade the antibody, and 2) the reducing environment of the cell extract, which could convert the trimeric and dimeric M204-scFv back to monomer, which we know to be a poor inhibitor of seeding. We conclude that further optimization of the M204-scFv is necessary to enhance its proteolytic and oligomeric stability.

M204 also recognizes oligomers, but not monomers or fibrils prepared from a number of amyloidgenic sequences, such as Aβ, α-synuclein, PrP(106-126), poly(Q)$_{40}$, and calcitonin, indicating that the epitope is a generic structure that is common among the oligomeric conformations of amyloid proteins (25). Similarly, antibodies enriched for binding to amyloid fibrils commonly recognize amyloid fibrils formed by different amyloidogenic proteins (31, 52), indicating that sequence-independent immunoreactivity is not rare, and may be evolved to protect against a broad spectrum of potentially pathological amyloids. Accordingly, conformational antibodies could be particularly effective therapeutic agents in Alzheimer's disease, in which mixed amyloid pathologies are common (53).

In summary, we engineered a single-chain, conformational antibody that recognizes recombinant oligomers of tau, and inhibits cell-to-cell seeding by extracts from autopsy sections from human donors with tau pathology. Aided by molecular structures of the scFv antibody that we determined, we anticipate that M204 could be a candidate for further protein engineering endeavors to produce antibodies as potential imaging agents and/or therapeutics.

Experimental procedures

Monoclonal M204 expression and purification

Hybridomas producing rabbit monoclonal M204 antibody were generated as described previously (25). Cells were maintained in Hybridoma-SFM (Gibco, catalog No. 1204-076) by seeding CELLine CL1000 bioreactor flasks (Argos, catalog No. 90005) with 20 million cells. After 1 week, antibody was purified from the filtered the media using a protein A column (Thermo Scientific, catalog No. 82080) pre-equilibrated with PBS. After washing with 20 column volumes of PBS, antibody was eluted with 100 mM glycine, pH 2.0, and neutralized with 1 M Tris–HCl, pH 9.0. The purified antibody fractions were collected and analyzed by SDS-PAGE (Fig. S6), buffer exchanged to 1× PBS with a 30-kDa cutoff ultracentrifugal spin filter (Amicon), and stored at −80 °C.

M204 antibody engineering, expression, and purification

The sequence encoding the variable regions of the heavy (VH) and light (VL) chains of M204 antibody were connected

Table 1

Data collection and refinement statistics

Statistics for the highest-resolution shells are shown in parentheses.

	Monomer_M204	Dimer_M204	Trimer_M204
Wavelength (Å)	0.7749	0.9792	0.9791
Resolution range	39.9-2.20 (2.26-2.20)	90.41-2.91 (2.99-2.91)	65.8-3.6 (3.69-3.60)
Space group	$P\,4_1\,2\,2$	$P\,2_1\,2_1\,2_1$	$P\,4_3\,2\,2$
Unit cell	60.4 60.4 159.4	60.6 105.3 176.5	60.2 60.2 526.4
	90 90 90	90 90 90	90 90 90
Total reflections	55,416 (4091)	93,397 (5737)	24,601 (1765)
Unique reflections	15,422 (1120)	25,041 (1651)	10,789 (795)
Multiplicity	3.6 (3.7)	3.7 (3.5)	2.3 (2.2)
Completeness (%)	97.9 (99.0)	98.0 (92.11)	87.4 (91.1)
Mean $I/\sigma\,(I)$	11.1 (1.9)	6.7 (1.2)	3.7 (0.9)
Wilson B-factor	41.2	56.9	72.0
R_{merge}	0.072 (0.644)	0.171 (0.975)	0.240 (0.923)
R_{meas}	0.084 (0.752)	0.198 (1.114)	0.276 (1.021)
R_{pim}	0.050 (0.435)	0.123 (0.722)	0.191 (0.712)
$CC_{1/2}$	99.9 (73.6)	98.8 (48.1)	95.2 (44.8)
Reflections used in refinement	15,417 (1,503)	25,026 (2,310)	9,710 (715)
Reflections used for R_{free}	1,542 (151)	2,504 (231)	1,079 (79)
R_{work}	0.194 (0.267)	0.186 (0.331)	0.252 (0.381)
R_{free}	0.235 (0.359)	0.238 (0.338)	0.283 (0.365)
Number of nonhydrogen atoms			
Macromolecules	1,707	6,790	5,103
Ligands	3	20	0
Solvent	104	32	0
Protein residues	226	899	675
RMS (bonds) (Å)	0.010	0.007	0.008
RMS (angles) (°)	1.1	1.2	1.50
Ramachandran favored (%)	94.6	95.5	95.2
Ramachandran allowed (%)	5.0	4.0	4.7
Ramachandran outliers (%)	0.4	0.6	0.2
Rotamer outliers (%)	2.7	6.6	0.15
Clashscore	1.78	2.84	3.38
Average B-factor (Å^2)			
Macromolecules	42.9	56.8	94.3
Ligands	51.0	101.	NA[1]
Solvent	44.5	39.6	NA

[1] NA, not applicable.

by a linker with sequence (Gly-Gly-Gly-Gly-Ser-Gly-Gly-Gly-Gly-Ser-Gly-Gly-Gly-Gly-Ser), and cloned into a pMES4 vector using the Gibson assembly method (54). The pMES4 vector encodes an N-terminal pelB signal peptide for periplasmic expression, and a His$_6$ tag at the C-terminal end. Protein expression and purification were performed according to our previous protocol (55). Briefly, *Escherichia coli* strain WK6 was transformed with the plasmid encoding M204-scFv and a fresh colony was picked and used to inoculate 10 ml of LB supplemented with ampicillin (100 mg/ml). The following day, the 10-ml pre-culture was used to inoculate 1 liter of TB media. Protein expression was induced by addition of isopropyl 1-thio-β-D-galactopyranoside at a final concentration of 1 mM at an OD = 0.6. M204-scFv was purified by IMAC after periplasmic lysis by using osmotic shock. Protein fractions from the IMAC were collected and purified on a HiLoad 16/600 Superdex 75 pg column in a running buffer of 20 mM Tris-HCl, pH 8.0, 150 mM NaCl. The protein concentration and purity was determined for the peaks corresponding to the M204-scFv monomer, dimer, and trimer from the size exclusion column, and aliquots of each were stored separately at −80 °C for further use.

Tau protein expression

Human WT tau-K18 (residues 244-372) and tau40 (residues 1-441) were expressed in a pNG2 and pET28b vectors, respectively, and purified as previously described (19, 56).

### Preparation and purification of tau oligomers

Recombinant tau-K18 at a concentration of 12 μM, or tau40 at a concentration of 50 μM were incubated in 1× PBS, pH 7.4, with 10 mM DTT and 2% ionic liquid (HR2-214-15, Hampton Research) with shaking for 16-18 h at 37 °C in a 96-well–plate (Thermo Scientific Nunc) with a plastic bead to enhance agitation. The solution was subsequently centrifuged for 5 min at 14,000 rpm to remove any large aggregates, and the supernatant was concentrated using an ultracentrifugal spin filter with a 10-kDa cutoff (Amicon). Concentrated samples were injected on a HiLoad 16/600 Superdex 75 pg (tau-K18), or Superose 6 Increase 10/300 GL (tau40).

ThT fluorescence assay

Tau-K18 was diluted to 25 μM in 1× PBS, pH 7.4, with 10 mM DTT, 10 μM ThT, and 2% ionic liquid (HR2-214-15, Hampton Research). Protein was aliquoted to 3 replicate wells of a 96-well–plate (Thermo Scientific Nunc), and plates were incubated at 37 °C for 20 h with shaking and a plastic bead to enhance agitation. Monomer, dimer, or trimer peaks of M204-scFv from SEC were added to tau at molar ratios of either 0.5:1 or 1:1. Aggregation was monitored by measuring ThT fluorescence at 440/480 nm excitation and emission wavelengths. Fibril kinetics were calculated by averaging reads from replicates in GraphPad Prism (GraphPad Software, Inc.), and error bars show the standard deviation of triplicate ThT measurements.
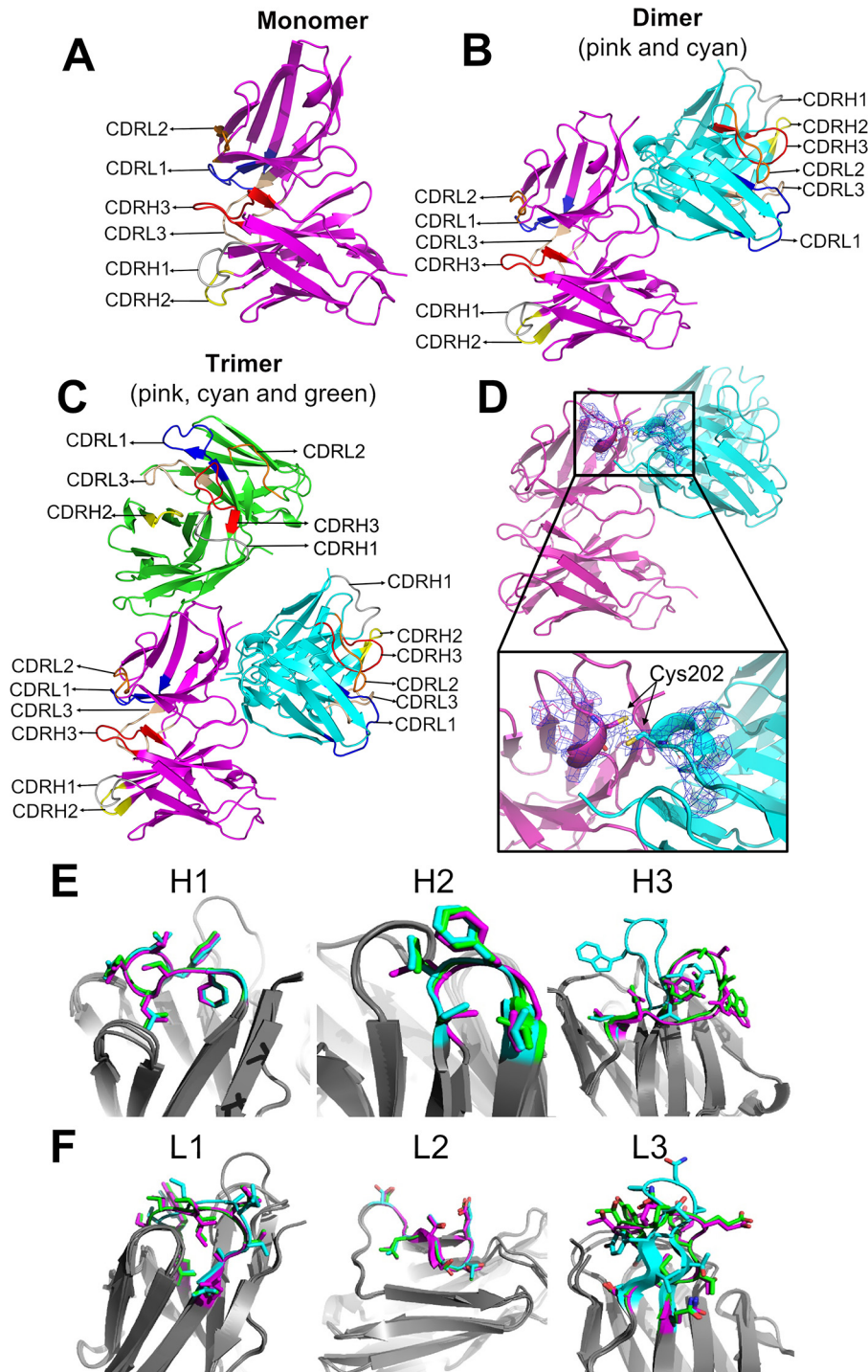
Figure 8. Crystal structures of M204-scFv monomer, dimer, and trimer antibodies. *A–C,* structures of M204-scFv monomer (*A*), dimer (*B*), and trimer (*C*), showing the positions of the complementarity-determining region (*CDR*) loops from the heavy (*H*) and light (*L*) chains. The structure of the M204-scFv monomer is colored *pink*, and in *B*, the dimer is formed between protomers colored *pink* and *cyan*. In *C*, the interaction of the protomers that form the dimer (colored in *pink* and *cyan*) is conserved, and a third protomer that interacts to form a trimer is colored in *green*. For each species in *A–C*, the CDR loops are solvent exposed, and oligomerization of the antibody could thus, in principle, enhance its interaction with the tau oligomer by polyvalent interactions. *D,* ribbon diagram of M204-scFv showing the electron density and proximity of cysteine 201 from two adjacent protomers, with the potential to form a disulfide bond (*yellow*). *E,* comparison of CDR loops from the heavy chains (*H1, H2,* and *H3*) of the M204-scFv monomer (*pink*), dimer (*cyan*) and trimer (*green*) species, and (*F*) CDR loops of the light chains (*L1, L2,* and *L3*) with the same coloring scheme.

ELISA

The surface of a 96-well–microplate (Greiner Bio-One, Germany) was coated with tau oligomer or monomer by incubating 100 μl of protein solution at a concentration of 1 μg/ml over-night at 4 °C in sodium bicarbonate buffer, pH 9.6. The following day, the plate was washed three times with TBST buffer (TBS, pH 7.6, and 0.1% Tween 20) and residual protein binding was blocked with 5% milk in TBST for 2 h at room temperature.

The same washing procedure was repeated between each of the subsequent steps. For the monoclonal M204-binding assay, 0.5 μg/well of monoclonal M204 in TBST supplemented with 2% milk was incubated with each well for 1 h at room temperature. Binding was detected with goat anti-rabbit HRP (Thermo Scientific), 100 μl/well, diluted 1:5000 in 2% milk/TBST. Finally, each well was washed three times with TBST buffer and HRP signal was produced by addition of 100 μl/well of 1-Step^{TM} Ultra TMB-ELISA Substrate (Thermo Scientific). Plates were incubated for 15 min at room temperature, HRP signal was quenched by addition of 2 M HCl. HRP signal was detected using a filter at 450 nm. In the case of M204-scFv, all steps were performed as described above except 5% milk was used for blocking, and HisProbe-HRP (Thermo Scientific, catalog No. 15165) was used for HRP detection at a dilution of 1:5000 in TBST.

Immunoblotting

Following SDS-PAGE, protein was transferred to a nitrocellulose membrane (Invitrogen) and detected by immunoblot analysis with rabbit polyclonal anti-oligomer A11 antibody (Invitrogen, catalog No. AHB0052). Followed by goat anti-rabbit HRP (Abcam, ab6721) as a secondary antibody. All membranes were developed using Pierce^{TM} ECL Plus substrate (Thermo Scientific, catalog No. 32132).

Crystallization

The M204-scFv monomer peak from SEC was concentrated to 9.6 mg/ml and crystallization trials were performed by mixing equal volumes of the protein and reservoir solution. Crystals appeared from cocktails containing 0.2 M lithium sulfate, 0.1 M phosphate/citrate, pH 4.2, and 20% (w/v) PEG 1000 (A6: JCSG-plus screen, Molecular Dimensions) after 3-7 days at 16 °C. The M204-scFv dimer peak was crystallized at 10 mg/ml from 0.15 M ammonium sulfate, 0.1 M MES, pH 6.0, 15% (w/v) PEG 4000 (B10: ProPlex screen, Molecular Dimensions). The M204-scFv trimer peak was crystallized at a concentration of 4.4 mg/ml from 0.1 M sodium acetate, pH 5.0, 1.5 M ammonium sulfate (F11: ProPlex screen, Molecular Dimensions). All crystals were cryoprotected with reservoir solution containing 35% (w/v) glycerol, and flash-frozen in liquid nitrogen.

X-ray data collection and structure solution

X-ray data were collected at beamlines 24-ID-C and 24-ID-E at the Advanced Photon Source at Argonne National Laboratories. Data were processed in XDS and XSCALE (57), and for the M204-scFv dimer, molecular replacement was performed using search model 5GS3 (chain H) in PHASER (58). Refinement and structure building was performed in PHENIX (59) and Coot (60). The M204-scFv trimer and monomer structures were solved using the coordinates from the M204-scFv dimer as a search model.

Tau biosensor cell maintenance and seeding

HEK293 cell lines stably expressing tau-K18 P301S-eYFP, referred to as "tau biosensor cells" were engineered by Marc Diamond's laboratory at UTSW (34) and used without further characterization or authentication. Cells were maintained in Dulbecco's modified Eagle's medium (Life Technologies, catalog No. 11965092) supplemented with 10% (v/v) FBS (Life Technologies, catalog No. A3160401), 1% penicillin/streptomycin (Life Technologies, catalog No. 15140122), and 1% Glutamax (Life Technologies, catalog No. 35050061) at 37 °C, 5% CO_2 in a humidified incubator. Fibrils and patient-derived seeds were incubated for 16 h with inhibitor to yield a final inhibitor concentration of 10 μM (on the biosensor cells). For seeding, inhibitor-treated seeds were sonicated in a cuphorn water bath for 3 min, and then mixed with 1 volume of Lipofectamine 3000 (Life Technologies, catalog No. 11668027) prepared by diluting 1 µl of Lipofectamine in 19 µl of OptiMEM. After 20 min, 10 µl of fibrils were added to 90 µl of tau biosensor cells. The number of seeded aggregates was determined by imaging the entire well of a 96-well–plate in triplicate using a Celigo Image Cytometer (Nexcelom) in the YFP channel. Aggregates were counted using ImageJ (61) by subtracting the background fluorescence from unseeded cells and then counting the number of peaks with fluorescence above background using the built-in Particle Analyzer. The number of aggregates was normalized to the confluence of each well, and dose-response plots were generated by calculating the average and standard deviations from triplicate measurements. For high quality images, cells were photographed on a ZEISS Axio Observer D1 fluorescence microscope using the YFP fluorescence channel.

Preparation of crude and Sarkosyl-insoluble brain-derived tau seeds

Tissue was received for neuropathlogically confirmed tauopathy cases from brain regions indicated in the figure legends. Tissue was cut into 0.2-0.3–g sections and then manually homogenized in a 15-ml ultra tissue grinder (Fisher 02-542-10) in 1 ml of 50 mM Tris, pH 7.4, with 150 mM NaCl containing 1× HALT protease. Samples were then sonicated in a cuphorn bath for 120 min with 30% power at 4 °C in a recirculating ice-water bath, according to Ref. 62, and were used for seeding without further purification.

For Sarkosyl-insoluble fibril fractions, 1-2 g of brain tissue were manually homogenized in 10 mM Tris–HCl, pH 7.4, 0.8 M NaCl, 10% sucrose, and 1× HALT protease inhibitor (Thermo) using a disposable ultra tissue grinder. After clarifying by centrifugation at 15,000 rpm for 10 min, Sarkosyl was added to the supernatant to a final concentration of 1% and incubated at 37 °C with shaking at 200 rpm for 1 h. Fibrils were pelleted by ultracentrifugation for 1 h at 80,000 rpm, and subsequently resuspended in 50 μl of PBS, pH 7.4, per gram of tissue.

Dot blot

Dot blots were prepared as described previously (63, 64).

Epitope mapping

Protein microarrays were constructed by conjugating biotinylated peptides on nitrocellulose-coated slides via NeutrAvidin, to produce a 65-kDa tetramer with exposed peptide epitopes.

Oligomer antibody inhibits seeding by AD brain-derived Tau

For microarray fabrication, a library of biotinylated amyloid peptides that were 12 residues with average molecular mass of 2 kDa were preincubated with NeutrAvidin (ThermoFisher Scientific, MA, USA) in PBS at a molar ratio of 4:1 for 1 h at room temperature with gentle agitation. The final concentration of peptide in the NeutrAvidin complex was 0.5 mg/ml. Tween 20 (T-PBS) was added to the peptide complex solution at a final concentration of 0.001%, and the solution was spotted onto a nitrocellulose-coated glass AVID slides (Grace Bio-Laboratory, Inc., OR, USA) using an Omni Grid 100 contact microarray printer (Genomic Solutions). One nanoliter of peptide solution was delivered to the membrane, corresponding ~0.5 ng of peptide per spot. Slides were stored in desiccator for further use.

Statistical analysis

Data were analyzed in GraphPad Prism by performing one-way analysis of variance (ANOVA) followed by a Tukey's multiple comparison test and a two-tailed unpaired multiple t test.

Data availability

Coordinates were submitted to the Protein Data Bank (PDB) with codes 6PIL for the M204-scFv monomer, 6PK8 for the dimer and 6PSC for the trimer.

References

1. Cova, I., Markova, A., Campini, I., Grande, G., Mariani, C., and Pomati, S. (2017) Worldwide trends in the prevalence of dementia. *J. Neurol. Sci.* **379,** 259–260 CrossRef Medline
2. Goedert, M., Wischik, C. M., Crowther, R. A., Walker, J. E., and Klug, A. (1988) Cloning and sequencing of the cDNA encoding a core protein of the paired helical filament of Alzheimer disease: identification as the microtubule-associated protein tau. *Proc. Natl. Acad. Sci. U.S.A.* **85,** 4051–4055 CrossRef Medline
3. Brier, M. R., Gordon, B., Friedrichsen, K., McCarthy, J., Stern, A., Christensen, J., Owen, C., Aldea, P., Su, Y., Hassenstab, J., Cairns, N. J., Holtzman, D. M., Fagan, A. M., Morris, J. C., Benzinger, T. L., *et al.* (2016) Tau and Aβ imaging, CSF measures, and cognition in Alzheimer's disease. *Sci. Transl. Med.* **8,** 338–366 CrossRef
4. Jackson, S. J., Kerridge, C., Cooper, J., Cavallini, A., Falcon, B., Cella, C. V., Landi, A., Szekeres, P. G., Murray, T. K., Ahmed, Z., Goedert, M., Hutton, M., O'Neill, M. J., and Bose, S. (2016) Short fibrils constitute the major species of seed-competent Tau in the brains of mice transgenic for human P301S Tau. *J. Neurosci.* **36,** 762–772 CrossRef
5. Ghetti, B., Oblak, A. L., Boeve, B. F., Johnson, K. A., Dickerson, B. C., and Goedert, M. (2015) Invited review: Frontotemporal dementia caused by microtubule-associated protein tau gene (MAPT) mutations: a chameleon for neuropathology and neuroimaging. *Neuropathol. Appl. Neurobiol.* **41,** 24–46 CrossRef Medline
6. Gao, Y. L., Wang, N., Sun, F. R., Cao, X. P., Zhang, W., and Yu, J. T. (2018) Tau in neurodegenerative disease. *Ann. Transl. Med.* **6,** 175 CrossRef Medline
7. Brundin, P., Melki, R., and Kopito, R. (2010) Prion-like transmission of protein aggregates in neurodegenerative diseases. *Nat. Rev. Mol. Cell Biol.* **11,** 301–307 CrossRef Medline
8. Cárdenas-Aguayo, M. D C., Gómez-Virgilio, L., DeRosa, S., and Meraz-Ríos, M. A. (2014) The role of tau oligomers in the onset of Alzheimer's disease neuropathology. *ACS Chem. Neurosci.* **5,** 1178–1191 CrossRef Medline
9. Tabaton, M., Mandybur, T. I., Perry, G., Onorato, M., Autilio-Gambetti, L., and Gambetti, P. (1989) The widespread alteration of neurites in Alzheimer's disease may be unrelated to amyloid deposition. *Ann. Neurol.* **26,** 771–778 CrossRef Medline
10. Hardy, J., and Selkoe, D. J. (2002) The amyloid hypothesis of Alzheimer's disease: progress and problems on the road to therapeutics. *Science* **297,** 353–356 CrossRef Medline
11. Ferreira, S. T., Vieira, M. N., and De Felice, F. G. (2007) Soluble protein oligomers as emerging toxins in Alzheimer's and other amyloid diseases. *IUBMB Life* **59,** 332–345 CrossRef Medline

12. Lasagna-Reeves, C. A., Castillo-Carranza, D. L., Sengupta, U., Clos, A. L., Jackson, G. R., and Kayed, R. (2011) Tau oligomers impair memory and induce synaptic and mitochondrial dysfunction in wild-type mice. *Mol. Neurodegener.* **6,** 39 CrossRef Medline

13. Lasagna-Reeves, C. A., Castillo-Carranza, D. L., Sengupta, U., Guerrero-Munoz, M. J., Kiritoshi, T., Neugebauer, V., Jackson, G. R., and Kayed, R. (2012) Alzheimer brain-derived tau oligomers propagate pathology from endogenous tau. *Sci. Rep.* **2,** 700 CrossRef Medline

14. Patterson, K. R., Remmers, C., Fu, Y., Brooker, S., Kanaan, N. M., Vana, L., Ward, S., Reyes, J. F., Philibert, K., Glucksman, M. J., and Binder, L. I. (2011) Characterization of prefibrillar Tau oligomers *in vitro* and in Alzheimer disease. *J. Biol. Chem.* **286,** 23063–23076 CrossRef Medline

15. Lasagna-Reeves, C. A., Castillo-Carranza, D. L., Sengupta, U., Sarmiento, J., Troncoso, J., Jackson, G. R., and Kayed, R. (2012) Identification of oligomers at early stages of tau aggregation in Alzheimer's disease. *FASEB J.* **26,** 1946–1959 CrossRef Medline

16. Fa, M., Puzzo, D., Piacentini, R., Staniszewski, A., Zhang, H., Baltrons, M. A., Li Puma, D. D., Chatterjee, I., Li, J., Saeed, F., Berman, H. L., Ripoli, C., Gulisano, W., Gonzalez, J., Tian, H., *et al.* (2016) Extracellular Tau oligomers produce an immediate impairment of LTP and memory. *Sci. Rep.* **6,** 19393 CrossRef Medline

17. Usenovic, M., Niroomand, S., Drolet, R. E., Yao, L., Gaspar, R. C., Hatcher, N. G., Schachter, J., Renger, J. J., and Parmentier-Batteur, S. (2015) Internalized Tau oligomers cause neurodegeneration by inducing accumulation of pathogenic Tau in human neurons derived from induced pluripotent stem cells. *J. Neurosci.* **35,** 14234–14250 CrossRef Medline

18. Combs, B., Tiernan, C. T., Hamel, C., and Kanaan, N. M. (2017) Production of recombinant tau oligomers *in vitro*. *Methods Cell Biol.* **141,** 45–64 CrossRef Medline

19. Seidler, P. M., Boyer, D. R., Rodriguez, J. A., Sawaya, M. R., Cascio, D., Murray, K., Gonen, T., and Eisenberg, D. S. (2018) Structure-based inhibitors of tau aggregation. *Nat. Chem.* **10,** 170–176 CrossRef Medline

20. Sievers, S. A., Karanicolas, J., Chang, H. W., Zhao, A., Jiang, L., Zirafi, O., Stevens, J. T., Münch, J., Baker, D., and Eisenberg, D. (2011) Structure-based design of non-natural amino-acid inhibitors of amyloid fibril formation. *Nature* **475,** 96–100 CrossRef Medline

21. Zheng, J., Liu, C., Sawaya, M. R., Vadla, B., Khan, S., Woods, R. J., Eisenberg, D., Goux, W. J., and Nowick, J. S. (2011) Macrocyclic β-sheet peptides that inhibit the aggregation of a tau-protein-derived hexapeptide. *J. Am. Chem. Soc.* **133,** 3144–3157 CrossRef Medline

22. Liu, C., Zhao, M., Jiang, L., Cheng, P. N., Park, J., Sawaya, M. R., Pensalfini, A., Gou, D., Berk, A. J., Glabe, C. G., Nowick, J., and Eisenberg, D. (2012) Out-of-register β-sheets suggest a pathway to toxic amyloid aggregates. *Proc. Natl. Acad. Sci. U.S.A.* **109,** 20913–20918 CrossRef Medline

23. Sawaya, M. R., Sambashivan, S., Nelson, R., Ivanova, M. I., Sievers, S. A., Apostol, M. I., Thompson, M. J., Balbirnie, M., Wiltzius, J. J., McFarlane, H. T., Madsen, A. O., Riekel, C., and Eisenberg, D. (2007) Atomic structures of amyloid cross-beta spines reveal varied steric zippers. *Nature* **447,** 453–457 CrossRef Medline

24. Castillo-Carranza, D. L., Sengupta, U., Guerrero-Muñoz, M. J., Lasagna-Reeves, C. A., Gerson, J. E., Singh, G., Estes, D. M., Barrett, A. D., Dineley, K. T., Jackson, G. R., and Kayed, R. (2014) Passive immunization with Tau oligomer monoclonal antibody reverses tauopathy phenotypes without affecting hyperphosphorylated neurofibrillary tangles. *J. Neurosci.* **34,** 4260–4272 CrossRef Medline

25. Kayed, R., Canto, I., Breydo, L., Rasool, S., Lukacsovich, T., Wu, J., Albay, R., 3rd, Pensalfini, A., Yeung, S., Head, E., Marsh, J. L., and Glabe, C. (2010) Conformation dependent monoclonal antibodies distinguish different replicating strains or conformers of prefibrillar Aβ oligomers. *Mol. Neurodegener.* **5,** 57 CrossRef Medline

26. Takekiyo, T., and Yoshimura, Y. (2018) Suppression and dissolution of amyloid aggregates using ionic liquids. *Biophys. Rev.* **10,** 853–860 CrossRef Medline

27. Takekiyo, T., Koyama, Y., Yamazaki, K., Abe, H., and Yoshimura, Y. (2013) Ionic liquid-induced formation of the α-helical structure of β-lactoglobulin. *J. Phys. Chem. B* **117,** 10142–10148 CrossRef Medline

28. Weaver, K. D., Vrikkis, R. M., Van Vorst, M. P., Trullinger, J., Vijayaraghavan, R., Foureau, D. M., McKillop, I. H., MacFarlane, D. R., Krueger, J. K.,

and Elliott, G. D. (2012) Structure and function of proteins in hydrated choline dihydrogen phosphate ionic liquid. *Phys. Chem. Chem. Phys.* **14,** 790–801 CrossRef Medline

29. Barghorn, S., and Mandelkow, E. (2002) Toward a unified scheme for the aggregation of tau into Alzheimer paired helical filaments. *Biochemistry* **41,** 14885–14896 CrossRef Medline

30. Karikari, T. K., Nagel, D. A., Grainger, A., Clarke-Bland, C., Hill, E. J., and Moffat, K. G. (2019) Preparation of stable tau oligomers for cellular and biochemical studies. *Anal. Biochem.* **566,** 67–74 CrossRef Medline

31. Kayed, R., Head, E., Sarsoza, F., Saing, T., Cotman, C. W., Necula, M., Margol, L., Wu, J., Breydo, L., Thompson, J. L., Rasool, S., Gurlo, T., Butler, P., and Glabe, C. G. (2007) Fibril specific, conformation dependent antibodies recognize a generic epitope common to amyloid fibrils and fibrillar oligomers that is absent in prefibrillar oligomers. *Mol. Neurodegener.* **2,** 18 CrossRef Medline

32. Kayed, R., Head, E., Thompson, J. L., McIntire, T. M., Milton, S. C., Cotman, C. W., and Glabe, C. G. (2003) Common structure of soluble amyloid oligomers implies common mechanism of pathogenesis. *Science* **300,** 486–489 CrossRef Medline

33. d'Abramo, C., Acker, C. M., Jimenez, H., and Davies, P. (2015) Passive immunization in JNPL3 transgenic mice using an array of phospho-Tau specific antibodies. *PLoS ONE* **10,** e0135774 CrossRef Medline

34. Kaufman, S. K., Sanders, D. W., Thomas, T. L., Ruchinskas, A. J., Vaquer-Alicea, J., Sharma, A. M., Miller, T. M., and Diamond, M. I. (2016) Tau prion strains dictate patterns of cell pathology, progression rate, and regional vulnerability *in vivo*. *Neuron* **92,** 796–812 CrossRef Medline

35. Nelson, A. L., and Reichert, J. M. (2009) Development trends for therapeutic antibody fragments. *Nat. Biotechnol.* **27,** 331–337 CrossRef Medline

36. Bird, R. E., Hardman, K. D., Jacobson, J. W., Johnson, S., Kaufman, B. M., Lee, S. M., Lee, T., Pope, S. H., Riordan, G. S., and Whitlow, M. (1988) Single-chain antigen-binding proteins. *Science* **242,** 423–426 CrossRef Medline

37. Saerens, D., Conrath, K., Govaert, J., and Muyldermans, S. (2008) Disulfide bond introduction for general stabilization of immunoglobulin heavy-chain variable domains. *J. Mol. Biol.* **377,** 478–488 CrossRef Medline

38. Wang, R., Xiang, S., Feng, Y., Srinivas, S., Zhang, Y., Lin, M., and Wang, S. (2013) Engineering production of functional scFv antibody in *E. coli* by co-expressing the molecule chaperone Skp. *Front. Cell Infect. Microbiol.* **3,** 72 CrossRef

39. Arndt, K. M., Muller, K. M., and Pluckthun, A. (1998) Factors influencing the dimer to monomer transition of an antibody single-chain Fv fragment. *Biochemistry* **37,** 12918–12926 CrossRef Medline

40. Griffiths, A. D., Malmqvist, M., Marks, J. D., Bye, J. M., Embleton, M. J., McCafferty, J., Baier, M., Holliger, K. P., Gorick, B. D., and Hughes-Jones, N. C. and (1993) Human anti-self antibodies with high specificity from phage display libraries. *EMBO J.* **12,** 725–734 CrossRef Medline

41. Serrano-Pozo, A., Frosch, M. P., Masliah, E., and Hyman, B. T. (2011) Neuropathological alterations in Alzheimer disease. *Cold Spring Harb. Perspect. Med.* **1,** a006189 CrossRef Medline

42. Xu, J. L., and Davis, M. M. (2000) Diversity in the CDR3 region of V(H) is sufficient for most antibody specificities. *Immunity* **13,** 37–45 CrossRef Medline

43. Arai, H., Glabe, C., and Luecke, H. (2012) Crystal structure of a conformation-dependent rabbit IgG Fab specific for amyloid prefibrillar oligomers. *Biochim. Biophys. Acta* **1820,** 1908–1914 CrossRef Medline

44. Sutton, K. A., Black, P. J., Mercer, K. R., Garman, E. F., Owen, R. L., Snell, E. H., and Bernhard, W. A. (2013) Insights into the mechanism of X-ray-induced disulfide-bond cleavage in lysozyme crystals based on EPR, optical absorption and X-ray diffraction studies. *Acta Crystallogr. D Biol. Crystallogr.* **69,** 2381–2394 CrossRef Medline

45. Weik, M., Ravelli, R. B., Kryger, G., McSweeney, S., Raves, M. L., Harel, M., Gros, P., Silman, I., Kroon, J., and Sussman, J. L. (2000) Specific chemical and structural damage to proteins produced by synchrotron radiation. *Proc. Natl. Acad. Sci. U.S.A.* **97,** 623–628 CrossRef Medline

46. Li, Z., Krippendorff, B. F., Sharma, S., Walz, A. C., Lavé, T., and Shah, D. K. (2016) Influence of molecular size on tissue distribution of antibody fragments. *MAbs* **8,** 113–119 CrossRef Medline

47. Day, E. S., Cote, S. M., and Whitty, A. (2012) Binding efficiency of protein–protein complexes. *Biochemistry* **51,** 9124–9136 CrossRef Medline

48. Goedert, M., Eisenberg, D. S., and Crowther, R. A. (2017) Propagation of Tau aggregates and neurodegeneration. *Annu. Rev. Neurosci.* **40,** 189–210 CrossRef Medline

49. Falcon, B., Zhang, W., Murzin, A. G., Murshudov, G., Garringer, H. J., Vidal, R., Crowther, R. A., Ghetti, B., Scheres, S. H. W., and Goedert, M. (2018) Structures of filaments from Pick's disease reveal a novel tau protein fold. *Nature* **561,** 137–140 CrossRef Medline

50. Falcon, B., Zivanov, J., Zhang, W., Murzin, A. G., Garringer, H. J., Vidal, R., Crowther, R. A., Newell, K. L., Ghetti, B., Goedert, M., and Scheres, S. H. W. (2019) Novel tau filament fold in chronic traumatic encephalopathy encloses hydrophobic molecules. *Nature* **568,** 420–423 CrossRef Medline

51. Hatami, A., Albay, R., 3rd, Monjazeb, S., Milton, S., and Glabe, C. (2014) Monoclonal antibodies against Aβ42 fibrils distinguish multiple aggregation state polymorphisms *in vitro* and in Alzheimer disease brain. *J. Biol. Chem.* **289,** 32131–32143 CrossRef Medline

52. O'Nuallain, B., and Wetzel, R. (2002) Conformational Abs recognizing a generic amyloid fibril epitope. *Proc. Natl. Acad. Sci. U.S.A.* **99,** 1485–1490 CrossRef Medline

53. James, B. D., Bennett, D. A., Boyle, P. A., Leurgans, S., and Schneider, J. A. (2012) Dementia from Alzheimer disease and mixed pathologies in the oldest old. *JAMA* **307,** 1798–1800 CrossRef Medline

54. Gibson, D. G., Young, L., Chuang, R. Y., Venter, J. C., Hutchison, C. A., 3rd, and Smith, H. O. (2009) Enzymatic assembly of DNA molecules up to several hundred kilobases. *Nat. Methods* **6,** 343–345 CrossRef Medline

55. Abskharon, R. N., Giachin, G., Wohlkonig, A., Soror, S. H., Pardon, E., Legname, G., and Steyaert, J. (2014) Probing the N-terminal β-sheet conversion in the crystal structure of the human prion protein bound to a nanobody. *J. Am. Chem. Soc.* **136,** 937–944 CrossRef Medline

56. Gustke, N., Steiner, B., Mandelkow, E. M., Biernat, J., Meyer, H. E., Goedert, M., and Mandelkow, E. (1992) The Alzheimer-like phosphorylation of tau protein reduces microtubule binding and involves Ser-Pro and Thr-Pro motifs. *FEBS Lett.* **307,** 199–205 CrossRef Medline

57. Kabsch, W. (2010) Xds. *Acta Crystallogr. D Biol. Crystallogr.* **66,** 125–132 CrossRef Medline

58. McCoy, A. J., Grosse-Kunstleve, R. W., Adams, P. D., Winn, M. D., Storoni, L. C., and Read, R. J. (2007) Phaser crystallographic software. *J. Appl. Crystallogr.* **40,** 658–674 CrossRef Medline

59. Adams, P. D., Afonine, P. V., Bunkóczi, G., Chen, V. B., Davis, I. W., Echols, N., Headd, J. J., Hung, L. W., Kapral, G. J., Grosse-Kunstleve, R. W., McCoy, A. J., Moriarty, N. W., Oeffner, R., Read, R. J., Richardson, D. C., *et al.* (2010) PHENIX: a comprehensive Python-based system for macromolecular structure solution. *Acta Crystallogr. D Biol. Crystallogr.* **66,** 213–221 CrossRef Medline

60. Emsley, P., Lohkamp, B., Scott, W. G., and Cowtan, K. (2010) Features and development of Coot. *Acta Crystallogr. D Biol. Crystallogr.* **66,** 486–501 CrossRef Medline

61. Schneider, C. A., Rasband, W. S., and Eliceiri, K. W. (2012) NIH Image to ImageJ: 25 years of image analysis. *Nat. Methods* **9,** 671–675 CrossRef Medline

62. Kaufman, S. K., Del Tredici, K., Thomas, T. L., Braak, H., and Diamond, M. I. (2018) Tau seeding activity begins in the transentorhinal/entorhinal regions and anticipates phospho-tau pathology in Alzheimer's disease and PART. *Acta Neuropathol.* **136,** 57–67 CrossRef Medline

63. Krotee, P., Rodriguez, J. A., Sawaya, M. R., Cascio, D., Reyes, F. E., Shi, D., Hattne, J., Nannenga, B. L., Oskarsson, M. E., Philipp, S., Griner, S., Jiang, L., Glabe, C. G., Westermark, G. T., Gonen, T., *et al.* (2017) Atomic structures of fibrillar segments of hIAPP suggest tightly mated β-sheets are important for cytotoxicity. *Elife* **6,** e19273 CrossRef

64. Krotee, P., Griner, S. L., Sawaya, M. R., Cascio, D., Rodriguez, J. A., Shi, D., Philipp, S., Murray, K., Saelices, L., Lee, J., Seidler, P., Glabe, C. G., Jiang, L., Gonen, T., and Eisenberg, D. S. (2018) Common fibrillar spines of amyloid-β and human islet amyloid polypeptide revealed by microelectron diffraction and structure-based inhibitors. *J. Biol. Chem.* **293,** 2888–2902 CrossRef Medline